

Surface Plastic Deformation by Sliding Elliptical Cylinder

Rostislav I. Nepershin

Plastic Deformation Systems Department, Moscow State University of Technology "STANKIN", Moscow, Russia
Email: nepershin_ri@rambler.ru

Received November 2014

Abstract

Steady state plastic flow of the ideal plastic half-space surface by sliding elliptical cylinder is numerically calculated with account of contact friction effect. Numerical solution of the plane strain hyperbolic differential equations with unknown contact pressure distribution is treated as nonlinear vector equation for the steady state plastic flow condition. Pronounced effect of the ellipse boundary curvature on the plastic flow mode is shown. Engineering application of the computer model is surface plastic deformation technology to improve wear and fatigue resistance of metal parts.

Keywords

Surface Layer, Plastic Flow, Ideal Plasticity, Sliding; Elliptical Cylinder, Friction

1. Introduction

Surface plastic deformation by rigid tools is used in engineering technology to increase wear and fatigue resistance of metal contact parts. Specification of technology parameters for surface plastic deformation is difficult engineering problem induced by complex elastic-plastic deformation of the surface layer.

Finite element analysis of rigid cylinder rolling along elastic-plastic half space is considered in [1] [2]. But large plastic deformation compared with the elastic one, unknown plastic region boundaries, stress and velocity singularities at the intersection of the toll contact with surface boundary are key problems for accuracy of the finite element elastic-plastic analysis.

Plastic deformation in surface layer, deems, is dominant factor of the surface plastic technology, and models on the base of ideal plasticity theory [3] [4] is reasonable. Steady state ideal plastic flow induced by rolling of rigid cylinder is considered in [5] using a small parameter approach. Approximate analysis related with the rolling friction is given in [6]. Steady state plastic flow of surface layer induced by rolling and sliding of circular cylinder is investigated in [7]-[9].

Present steady state plastic flow model of surface layer is developed for rigid elliptical cylinder sliding with contact friction consideration. Variable curvature and ellipse orientation relative the surface boundary are effective features of the plastic flow mode. Sliding of the wedge [10] and circular cylinder [7]-[9] along the plastic surface are limit cases of the present model.

2. Problem Formulation

Steady state plastic flow of an ideal plastic half-space surface layer induced by sliding of loaded long elliptical cylinder is considered. Plane strain plastic flow on the plane x, y orthogonal to the cylinder axis is assumed with half-space moving velocity V and nonmoving cylinder.

Stresses and velocities in the plastic region, loads and torque applied to the cylinder are non-dimension, using material plastic constant $2k$ and sliding velocity V as reference units. Elliptical section of the cylinder and scheme of the plastic region are shown in **Figure 1**.

Steady state plastic region OAB and cylinder are non- moving in coordinates x, y with the origin O at the lower contact point of the cylinder with half-space boundary. First principal axis x_1 of the ellipse is inclined at the angle θ_0 to the axis x . Minimal half-length of the ellipse axis is assumed as unit reference length, and ellipse form is defined by non-dimensional maximal half-length axis a . Ellipse boundary with the center C can be written in parametric form in principal ellipse coordinates x_1, x_2

$$x_1 = a \cos \omega, y_1 = \sin \omega, -\pi/2 \leq \omega \leq \pi/2 \quad (1)$$

Tangent angle θ to the axis x_1 at the point x_1, x_2 is defined as follows

$$\operatorname{tg} \theta = -(\operatorname{ctg} \omega)/a \quad (2)$$

Coordinates x, y of the ellipse point x_1, x_2 are defined by shift and rotation transformation of the axes

$$\begin{aligned} x &= x_C + x_1 \cos \theta_0 - y_1 \sin \theta_0 \\ y &= y_C - x_1 \sin \theta_0 + y_1 \cos \theta_0 \end{aligned} \quad (3)$$

Angle θ_0 at the point O is defined from Equation (2) by specified parameter ω_0 . Coordinates x_C, y_C of the ellipse center C are found from Equations (1) and (3) with specified ω_0 using the condition $x = y = 0$

$$\begin{aligned} x_C &= \sin \omega_0 \sin \theta_0 - a \cos \omega_0 \cos \theta_0, \\ y_C &= a \cos \omega_0 \sin \theta_0 - \sin \omega_0 \cos \theta_0. \end{aligned} \quad (4)$$

Contact boundary OA is defined by specified parameter ω_A for the point A . Coordinates x, y of the boundary OA with the tangent angle α to the axis x

$$\alpha = \theta - \theta_0, \omega_0 \leq \omega \leq \omega_A \quad (5)$$

are defined by Equations (1)-(3).

Parameters ω_0, ω_A and a define ellipse form, the angle θ_0 and contact boundary OA on different segments of the ellipse. Length of the contact boundary l_c is defined by integral

$$l_c = \int_{\omega_0}^{\omega_A} [\cos^2 \omega + a^2 \sin^2 \omega]^{1/2} d\omega \quad (6)$$

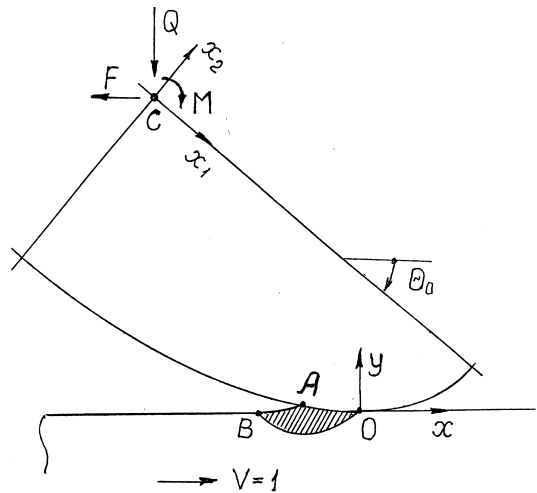


Figure 1. Steady state surface plastic region.

Boundary OA with contact pressure and shear stress define loads Q , F and torque M (**Figure 1**) using static equilibrium of the cylinder.

Plane strain plastic flow of the ideal plastic material [3] [4] is defined by hyperbolic differential Equations with orthogonal ζ and η slip lines

$$dx/dy = \operatorname{tg}\varphi \text{ for } \zeta, dx/dy = -\operatorname{ctg}\varphi \text{ for } \eta, \quad (7)$$

Henky's Equations for the mean stress σ and angle φ

$$d\sigma - d\varphi = 0 \text{ along } \zeta, d\sigma + d\varphi = 0 \text{ along } \eta \quad (8)$$

where $2k = 1$ is used as unit stress, and Geiringer's Equations for the velocity projections V_ζ , V_η on the slip lines

$$dV_\zeta - V_\eta d\varphi = 0 \text{ along } \zeta, dV_\eta + V_\zeta d\varphi = 0 \text{ along } \eta \quad (9)$$

Stress and velocity components in coordinates x , y are related with σ , φ , V_ζ and V_η variables by Equations

$$\sigma_x = \sigma - 0.5\sin 2\varphi, \sigma_y = \sigma + 0.5\sin 2\varphi, \tau_{xy} = 0.5\cos 2\varphi \quad (10)$$

and

$$V_x = V_\zeta \cos\varphi - V_\eta \sin\varphi, V_y = V_\zeta \sin\varphi + V_\eta \cos\varphi \quad (11)$$

3. Boundary Conditions

Stress free boundary AB (**Figure 2**) is the stream line of the steady state plastic flow, with the principal stresses $\sigma_1 = 0$, $\sigma_2 = -1$ along this boundary, and we have stress and velocity boundary conditions on AB

$$\sigma = -0.5, V_\zeta + V_\eta = 0 \quad (12)$$

Friction on the boundary AO is specified by contact shear stress $0 \leq \tau_c \leq 0.5$, used in technological plasticity problems with large contact pressures [11]. Incline angle γ for the η slip line on the contact boundary (**Figure 2(a)**) is found from third Equation (10) using specified τ_c value

$$\gamma = 0.5\cos^{-1}(2\tau_c) \quad (13)$$

Angle φ between the ζ slip lines and axis x on the boundary AO with the tangent angles α is defined as

$$\varphi = \pi/2 + \gamma - \alpha, 0 \leq \alpha \leq \alpha_A \quad (14)$$

Zero normal component of the velocity and the angle γ define boundary condition for the velocities V_ζ and V_η on the boundary AO

$$V_\zeta - V_\eta \operatorname{tg}\gamma = 0 \quad (15)$$

Half-space velocities $V_x = 1$, $V_y = 0$ are continues on the rigid-plastic boundary OB , and from Equations (11) it follows

$$V_\zeta = \cos\varphi, V_\eta = -\sin\varphi \quad (16)$$

Mean stress σ_O at the point O is defined from second Equation (8) for the η slip line, using first boundary condition (12) with $\varphi = \pi/4$ at the point B , and Equation (14) with $\alpha = 0$ at the point O

$$\sigma_O = -(0.5 + \gamma + \pi/4) \quad (17)$$

Fun angle ψ for the ζ slip lines at the singular point A with tangent angle β on the stress free boundary AB is found using Equation (14) with $\alpha = \alpha_A$

$$\psi = \pi/4 + \gamma - (\alpha_A + \beta) \quad (18)$$

Angle β is defined during problem solution using condition $y = 0$ at the point B .

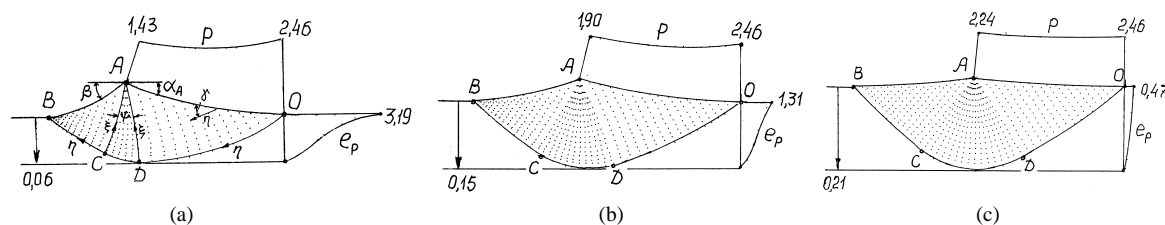


Figure 2. Plastic regions with pressure and plastic. Strain distributions for variants (a) 1; (b) 2 and (c) 3 in **Table 1**.

Limit value α_A^* for the steady state plastic flow is found from Equation (18) with $\psi = 0$

$$\alpha_A^* = \pi/4 + \gamma - \beta \quad (19)$$

Corresponding limit parameter ω_A^* and contact length l_c are found from Equations (5) and (6).

4. Numerical Solution

Numerical solution of the problem with specified parameters a , ω_O , ω_A and τ_c begins by initial guess for the angle β with constrain $\alpha_A < \alpha_A^*$ in Equation (19).

Then mean stress σ_A at the singular point A on the contact boundary AO is found from boundary condition (12) and second Equation (8) for the η slip line

$$\sigma_A = -(0.5 + \psi) \quad (20)$$

Fan angle ψ is defined by Equation (18) with the angle α_A found from Equations (2) and (5) for specified parameters a , ω_O and ω_A .

Initial mean stress distribution σ_i is specified at the nodes $i = 1, 2, 3, \dots, N$ on the contact boundary AO proportional the angles α_i , defined by the parameters ω_i in the interval $\omega_O \leq \omega_i \leq \omega_A$. Mean stress σ_i distribution, boundary condition (14) for the angles φ_i and contact boundary AO , defined by Equations (1) and (3), specify Cauchy's boundary value problem for differential Equations (7) and (8).

Cauchy's problem is solved using numerical procedures [11] with the result of slip lines with σ , φ variables calculation in the region AOD (**Figure 2(a)**). Then σ and φ variables are specified at the singular point A using second Equation (8), followed by numerical solution of Riemann's problem in the region ADC with known σ , φ variables on the slip line AD . Finally, inverse Cauchy's problem is solved numerically in the region ACB , using known σ , φ variables on the slip line AC with $\sigma = -0.5$ on calculated stress free boundary AB . Then initial guess for the angle β is corrected to satisfy condition $y = 0$ at the point B .

So, slip lines in the plastic region are calculated for specified stress σ distribution on the contact boundary AO . Next procedure is numerical calculation of the velocity field in the plastic region using conditions (15) on the boundary AO and (16) on the boundary OB . First, velocities V_ξ , V_η are calculated in the region AOD by numerical solution of the mixed boundary value problem for Equations (9) with known φ angles at the slip line nodes. Then velocity field is calculated in the region ADC from Riemann's problem with known V_ξ , V_η on the slip lines AD and CD , followed by velocity field calculation in the region ACB , using known V_ξ , V_η on the slip lines AC and CB , with the result of V_ξ and V_η calculation on the stress free boundary AB .

Velocities V_ξ and V_η must satisfy steady state plastic flow condition in Equation (12). If we define specified σ_i values on the boundary AO as the vector σ in N dimension space and values

$$f_i = (V_\xi + V_\eta)_i \quad (21)$$

at the N nodes of the boundary AB as the vector function f in the same N dimension space, then we have nonlinear vector Equation (22) for the steady state plastic flow problem solution

$$f(\sigma) = 0 \quad (22)$$

because numerical procedures for calculation of the slip lines and velocity field in the plastic region give unique relation between vectors σ and f . Equation (22) with $N \leq 20$ was solved using numerical procedures [12] for Broyden's method [13].

Equation (22) is solved with accuracy $\max f_i \leq 10^{-3}$.

Then contact pressure distribution

$$p_i = -(\sigma_i - 0.5 \sin 2\gamma) \quad (23)$$

was calculated on the boundary AO , followed by integration of pressure and contact shear stresses to find loads Q , F and torque M (**Figure 1**).

5. Numerical Results

For numerical solution of the problem FORTRAN program was written with input parameters a , τ_c , ω_O , ω_A and output data in the form of tables and graphical mapping of the slip line nodes as pixels on the monitor screen. Stream lines in the plastic region with accumulated plastic strain e_p and orthogonal grid distortions were calculated using numerical procedures in [14].

Numerical examples below were calculated for the ellipse parameter $a = 2$, three variants of the pairs $\{\omega_O, \omega_A\}$ and three typical values τ_c for practical surface plastic deformation technology to illustrate variable contact curvature and friction effects.

Three variants of the ellipse contact boundary AO , defined by the parameters ω_O and ω_A , are given in **Table 1**. Corresponding ellipse incline angle θ_O , tangent angle α_A at the point A , ellipse center C and contact length l_c are calculated from Equations (2), (4), (5) and (6). In variants 1 to 3 the incline angles θ_O and contact angles α_A are decreased with decrease of the ellipse curvature and increase of the contact length l_c .

Calculated slip lines in the plastic region with distributions of contact pressure p and accumulated plastic strain e_p of the material at the exit from the plastic region with shear contact stress $\tau_c = 0.1$ are shown in **Figure 2** for the ellipse boundary variants in **Table 1**. Curvature decrease of the ellipse contact boundary results in more homogeneous contact pressure distribution and decrease of the gradient and value of the plastic strain distributions through thickness of the surface plastic layer. But mean contact pressure is increased, and for smooth boundary with $\tau_c = 0$ it is approached to Prandtl's flat punch value $p = 1 + \pi/2$.

Velocity hodographs on the plane V_x, V_y in the plastic regions in **Figure 2** are presented in **Figure 3** for the same three variants of the ellipse contact boundary (**Table 1**) and shear contact stress $\tau_c = 0.1$. Velocities V_x, V_y are calculated using Equations (11) with known variables V_ξ, V_η, φ at the slip line nodes and mapped by pixels on the monitor screen.

Unit velocity vector at the point B is decreased along the stress free boundary AB with tangent angle increase to the β at the point A . Then velocity vector direction is rotated at the singular point A to the tangent angle α_A at the contact boundary, followed by increase of the vector module tangent to the boundary AO from the point A to the point O where it is unit horizontal vector.

Boundary $BCDO$ of the plastic region on the plane x, y (**Figure 2**) is mapped to the point $BCDO$ on the hodograph plane (**Figure 3**), as the result of the velocity continuity with moving half-space given by Equations (16).

Curvature decrease of the ellipse boundary AO from variant 1 to 3 in **Table 1**, and from (a) to (c) in **Figure 2** and **Figure 3** results in drastic velocity field non-homogeneous decrease, with homogeneous velocity field $V_x = 1, V_y = 0$ for the flat sliding Prandtl's punch.

Initial orthogonal grid distortions with the stream lines for the plastic regions in **Figure 2** are shown in **Figure 4** for the same variants of the ellipse contact boundaries in **Table 1**. Plastic boundary OB with the half-space is shown by dash line.

Movement of material point along the stream lines is calculated using steady state velocity fields in **Figure 3** for constant horizontal displacement increment dx at the entry to the plastic regions.

Displacement of the material point along the stream lines in the plastic region is calculated using mean velocity vectors in the "time" interval dx , because the half-space velocity is unit.

Final displacement Δx is defined by the slow material point, moving on the path BAO , while the fast material point is moved with unit velocity on horizontal path tangent to the boundary of the plastic region. Calculated positions of the material points on the stream lines are mapped on the monitor screen by pixels at each displacement increments dx .

Increase of the ellipse contact boundary from variant 3 to 1 in **Table 1** and from (c) to (a) in **Figure 4** results in drastic grid distortion and thickness decrease of the surface plastic layer.

Contact shear stress effect on the pressure at the points O and A , loads Q and F , torque M , surface plastic layer thickness h_p and maximum plastic strain e_p is given in **Table 2** for the three variants of the ellipse contact boundary in **Table 1**.

Numerical results in **Table 2** show essential effect of the ellipse contact curvature on the surface plastic flow. Contact friction decrease results in homogeneous plastic strain distribution through the surface plastic layer.

Table 1. Variants of the ellipse contact boundary.

Variant	$-\omega_O$	$-\omega_A$	$-\theta_O$	$-x_C$	y_C	α_A	l_c
1	0.05	0.26	1.47	0.15	1.99	0.39	0.22
2	0.50	0.75	0.74	0.97	1.54	0.25	0.36
3	1.10	1.30	0.25	0.66	1.09	0.11	0.38

Table 2. Contact friction effect on the surface plastic deformation by sliding elliptical cylinder.

Variant	τ_c	p_o	p_A	Q	F
1	0.10	1.43	2.46	0.41	0.10
	0.05	1.49	2.52	0.42	0.09
	0.00	1.57	2.57	0.44	0.08
	0.10	1.90	2.46	0.75	0.13
2	0.05	1.96	2.52	0.78	0.12
	0.00	2.01	2.57	0.80	0.10
	0.10	2.24	2.46	0.89	0.09
	0.05	2.30	2.52	0.91	0.07
3	0.00	2.35	2.57	0.93	0.05

Variant	τ_c	M	h_p	max e_p
1	0.10	0.22	0.06	3.19
	0.05	0.20	0.07	2.74
	0.00	0.18	0.08	2.40
	0.10	0.81	0.15	1.31
2	0.05	0.80	0.16	1.20
	0.00	0.80	0.17	1.11
	0.10	0.51	0.20	0.47
	0.05	0.50	0.22	0.43
3	0.00	0.49	0.23	0.41

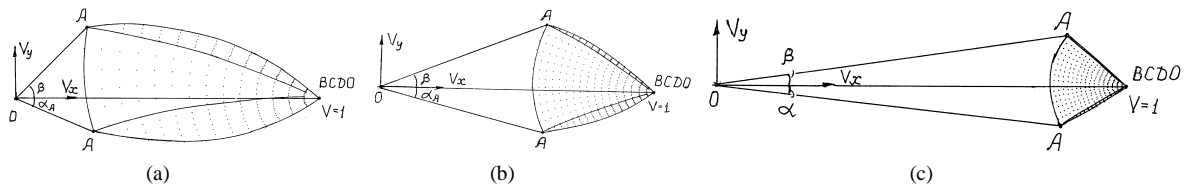


Figure 3. Velocity hodographs for the plastic regions (a), (b), (c) in **Figure 2**.

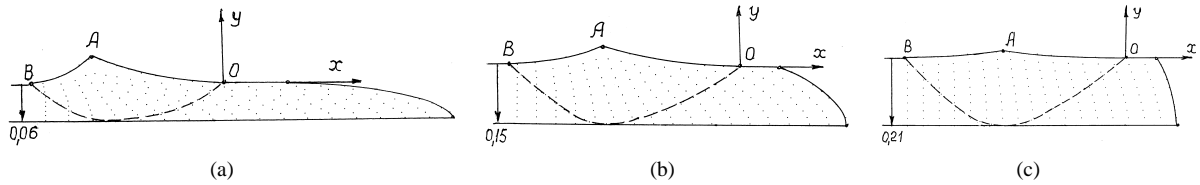


Figure 4. Stream lines with grid distortions for the plastic regions (a), (b), (c) in **Figure 2**.

Dimensional values of the ellipse center coordinates, contact length and plastic layer thickness are defined by multiplication of non-dimensional values on dimension value of the minor ellipse half-length b . Dimension shear stress τ_c and pressures p are defined by multiplication of non-dimensional values on double plastic constant $2k$, where $k = \sigma_Y/2$ for Tresca, or $k = \sigma_Y/\sqrt{3}$ for Mises yield criterion. The material yield stress σ_Y should be specified using compression stress-strain curve in the range of mean plastic strains in **Figure 2** and in **Table 2**, to approximate material work hardening effect.

6. Conclusions

Surface steady state plastic deformation by sliding elliptical cylinder with contact friction effect is modeled using hyperbolic differential equations of the plane strain ideal plasticity theory.

Plastic region with curved stress free boundary is calculated by numerical solution of nonlinear vector equation with unknown contact pressure distribution. Numerical results show essential effect of the ellipse contact boundary curvature on the mode of the surface plastic flow. Curvature of the contact boundary can be changed by rotation of the ellipse principal axes relative the surface boundary.

Numerical model is performed by FORTRAN program to investigate effects of the ellipse form, curvature and length of contact boundary and contact friction on the plastic flow of the surface with contact pressure and plastic strain distributions, loads and torque applied to the cylinder. These results, deems, are useful for engineering problems of metal parts surface plastic deformation to increase wear and fatigue resistance.

Acknowledgements

Russian Federation Ministry of Education and Science support by project No. 9.2445.2014/K is gratefully acknowledged.

References

- [1] Howell, M., Hahn, G.T., Rubin, C.A. and McDowell, D.L. (1995) Finite Element Analysis of Rolling Contact for Non-linear Kinematic Hardening Bearing Steel. *Journal of Tribology*, **117**, 729-736. <http://dx.doi.org/10.1115/1.2831544>
- [2] Shiratori, M., Ito, M. and Hashimoto, M. (1995) Elastic-Plastic Analysis of Rolling Contact for Surface Hardened Steel. *Trans. Jap. Soc. Mech. Eng. A.*, **61**, 1064-1069. <http://dx.doi.org/10.1299/kikaia.61.1064>
- [3] Hill, R. (1985) *The Mathematical Theory of Plasticity*. 11th Edition, Oxford University Press, Oxford.
- [4] Ishlinsky, A.Yu. and Ivlev, D.D. (2001) *The Mathematical Theory of Plasticity*. FIZMATLIT, Moscow.
- [5] Marshall, E.A. (1968) Rolling Contact with Plastic Deformation. *Journal of the Mechanics and Physics of Solids*, **16**, 243-254. [http://dx.doi.org/10.1016/0022-5096\(68\)90032-X](http://dx.doi.org/10.1016/0022-5096(68)90032-X)
- [6] Collins, I.F. (1972) A Simplified Analysis of the Rolling of Cylinder on a Rigid/Perfectly Plastic Half-Space. *International Journal of Mechanical Sciences*, **14**, 1-14. [http://dx.doi.org/10.1016/0020-7403\(72\)90002-1](http://dx.doi.org/10.1016/0020-7403(72)90002-1)
- [7] Nepershin, R.I. (2002) On Rolling and Sliding of a Cylinder along a Perfectly Plastic Half-Space with Allowance for Contact Friction. *Doklady Physics*, **47**, 256-259. <http://dx.doi.org/10.1134/1.1467875>
- [8] Nepershin, R.I. (2003) The Rolling and Slipping of a Cylinder along the Boundary of an Ideally Plastic Half-Space. *Journal of Applied Mathematics and Mechanics*, **67**, 293-301. [http://dx.doi.org/10.1016/S0021-8928\(03\)90015-3](http://dx.doi.org/10.1016/S0021-8928(03)90015-3)
- [9] Nepershin, R.I. (2013) Plastic Deformation of Surface Layer during Rigid Cylinder Rolling and Sliding. *Journal of Friction and Wear*, **34**, 204-207. <http://dx.doi.org/10.3103/S1068366613030112>
- [10] Nepershin, R.I. (2001) On Sliding of Obtuse Wedge along the Boundary of a Perfectly Plastic Half-Space. *Doklady Physics*, **46**, 885- 887. <http://dx.doi.org/10.1134/1.1433536>
- [11] Druyanov, B.A. and Nepershin, R.I. (1994) *Problems of Technological Plasticity*. Elsevier, Amsterdam.
- [12] Dennis, J.E. and Shnabel, R.B. (1983) *Numerical Methods for Unconstrained Optimization and Nonlinear Equations*. Prentice-Hall, Englewood Cliffs.
- [13] Broyden, C.G. (1965) A Class of Methods for Solving Nonlinear Simultaneous Equations. *Maths. Comp.*, **19**, 577-593.
- [14] Nepershin, R.I. (2004) Rolling and Sliding of Rigid Cylinder along the Boundary of a Rigid-Plastic Half-Space. *Mechanics of Solids*, **39**, 81-93.